Available online at www.sciencedirect.com
SCIENCE DIRECT®
Journal of Sound and Vibration 271 (2004) 635–649
JOURNAL OF SOUND AND VIBRATION
www.elsevier.com/locate/jsvi

An analytical investigation of single actuator and error sensor control in connected plates

John Keir[a,*], Nicole J. Kessissoglou[a], Chris J. Norwood[b]

[a] *School of Engineering, James Cook University, Townsville, Qld 4811, Australia*
[b] *Aeronautical and Maritime Research Laboratory (AMRL), Defence Science and Technology Organisation (DSTO), Melbourne, Vic 3001, Australia*

Received 10 January 2002; accepted 10 March 2003

Abstract

Vibrations in structures travel in the form of flexural and extensional waves, and transfer energy to other components of the system coupled to the structure. This may result in an undesirable system response or sound radiation. This paper presents an analytical and computational investigation of active control of the dynamic response characteristics of a series of rectangular plates coupled together and subject to point force excitation. The idealized periodic point force may represent the actions of vibrating mounted machinery such as motors or engines. Feedforward active control of the flexural waves in the plate configurations is applied to actively attenuate the structural response. It is shown that for L, T and cross-shaped plates, global attenuation may be achieved using a single control source and a single error sensor.

1. Introduction

Considerable attention has been given to the study of wave propagation through coupled plate structures in an L, T or cross configuration in the past few decades as they are often found in the maritime and building industries [1–7]. Kim et al. [1] analytically investigated the effect of in-plane modes on structure-borne noise propagation in ship structures. The wave amplitudes were determined by using the boundary conditions, continuity equations and taking into account the bending, shearing and longitudinal effects at the corner junction. Shen and Gibbs [2] described an approximate solution for the bending vibrations of a combination of rectangular thin plates. It was shown that the structural response was a function of the force input position, forcing

*Corresponding author.
E-mail address: john.keir@jcu.edu.au (J. Keir).

0022-460X/03/$ - see front matter
doi:10.1016/S0022-460X(03)00285-2

frequency, material parameters and edge constraints. Budrin and Nikiforov [3] investigated the transmission of flexural and extensional waves normally incident to the corner junction in T and cross-shaped plates. The energy reflection and transmission coefficients, and the frequency response for the plates configurations were determined. It was shown that as the frequency is increased, the extensional reflection coefficient decreases. Therefore, the amount of energy transmitted through the joint as flexural and extensional waves increases. In general, the effect on the transmission of bending and in-plane waves through the junction of semi-infinite and finite plates is well understood [4–7]. This includes the effects from the bending rigidity, material density and loss factors on the transmission.

Although there has been much work on active control of single beams and plates, there has been very little work on active control of connected plates [8]. This paper is a theoretical investigation on the active control of plates connected at right angles. The theory is presented for a generic structure consisting either of 2, 3 or 4 plates corresponding to an L, T or cross-shape, respectively. An active control system composing of a single actuator and single error sensor is applied to the connected plates, and the global response is observed.

2. Theory

The theory is presented for a generic structure consisting of four finite plates joined together at right angles in a cross-shape. The geometry of the plates and the alignment of the co-ordinate system are shown in Fig. 1. For mathematical simplicity, all four plates are simply supported

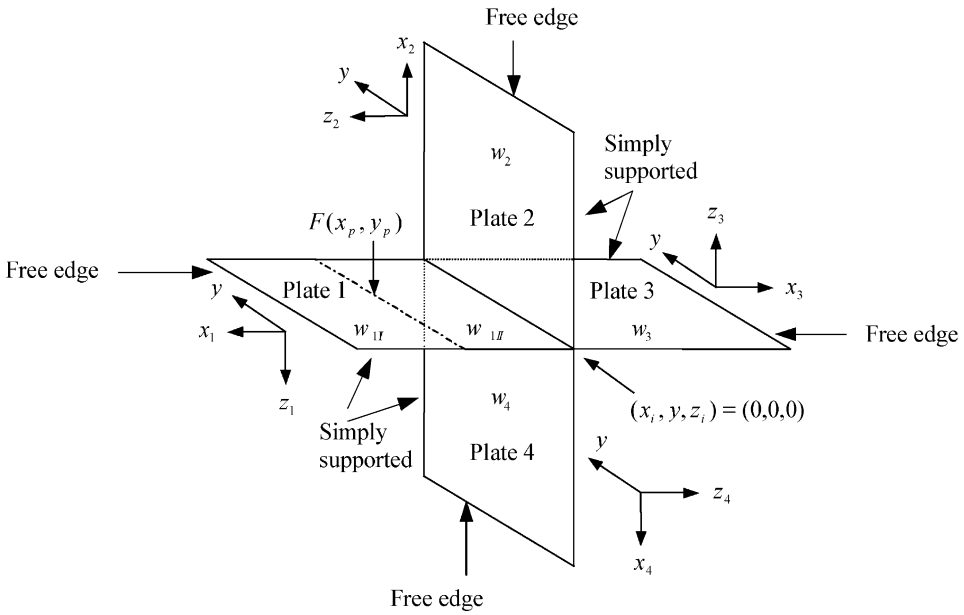

Fig. 1. Finite cross-shaped plate under point force excitation, showing the five regions of the coupled structure, the boundary conditions and the sign convention.

along edges $y = 0$ and L_y and are free at the other ends corresponding to $x_i = L_{xi}$ for i= 1–4. The junction of the four plates coincides with $x_i = 0$.

As the plate is simply supported along $y = 0$ and L_y, a modal solution in the y-direction can be obtained to describe the structural response. Due to the free edges, a travelling wave solution is used to describe the displacement in the x-direction. The disturbing force is analytically modelled by a point force excitation at (x_p, y_p). The forcing function of magnitude F_p can be described by the Dirac delta function

$$F(x, y) = F_p\delta(x - x_p)\delta(y - y_p). \tag{1}$$

The cross-shaped plate can be separated into five sections, as shown in Fig. 1. Note that on plate 1, the primary displacement $w_1^p(x_1, y)$ is separated into two components $w_{1I}^p(x_1, y)$ and $w_{1II}^p(x_1, y)$ due to the external driving force. The plate primary flexural displacement in the various sections can be described by

$$w_i^p(x_i, y) = \sum_{m=1}^{\infty}(A_i e^{-jk_x x_i} + B_i e^{jk_x x_i} + C_i e^{-k_n x_i} + D_i e^{k_n x_i}) \sin k_y y, \quad i = 1 - 4, \tag{2}$$

where A_i and B_i are coefficients of the propagating waves, and C_i and D_i are coefficients of the near-field decay waves. $k_x = \sqrt{k_p^2 - k_y^2}$ is the propagating wave number in the x-direction, and $k_n = \sqrt{k_p^2 + k_y^2}$ is the decaying wave number in the x-direction. $k_p = \sqrt{\omega}(\rho h/D)^{1/4}$ is the plate bending wave number, where $D = Eh^3/12(1 - v^2)$ is the plate flexural rigidity, E is Young's modulus, h is the plate thickness, v is the Poisson ratio and ρ is the density. $k_y = m\pi/L_y$ is the wave number in the y-direction, where $m = 1, 2, 3 \ldots \infty$ is the mode number. For plates of the same material properties, lengths and thicknesses, the various structural wave numbers are the same for each plate. For a T-shaped structure, plate 4 and $w_4^p(x_4, y)$ are eliminated, and similarly, for an L-shaped plate, plates 3 and 4, and therefore $w_3^p(x_3, y)$ and $w_4^p(x_4, y)$ are not required.

It is evident that 12, 16 and 20 unknown constants must be evaluated if the structural response is to be calculated for an L, T and cross-plate configuration, respectively. These can be found using boundary equations at the free edges $x_i = L_{xi}$ for zero bending moment and net vertical shear force [9]. At the driving force location of (x_p, y_p), four coupling equations are used to describe the continuity of the plate response under forced excitation [10]. The continuity relationships correspond to the continuity of the plate displacement, slope, moment and shear force. The boundary conditions at the structural junction of the coupled plates corresponding to $(x_i, z_i) = (0, 0)$ must also satisfy continuity of plate displacement, slope, moment and shear force. Using the sign convention outlined in Fig. 1, Eqs. (3) and (4) correspond to the continuity of the plate displacement while Eq. (5) corresponds to the continuity of plate slope at the junction. Eqs. (6)–(8) describe the equilibrium of forces and moments at the junction.

$$-w_{1II} = u_2 = w_3 = -u_4, \tag{3}$$

$$-u_1 = -w_2 = u_3 = w_4, \tag{4}$$

$$\frac{\partial w_{1II}}{\partial x_1} = \frac{\partial w_2}{\partial x_2} = \frac{\partial w_3}{\partial x_3} = \frac{\partial w_4}{\partial x_4}, \tag{5}$$

$$Q_{x1} - N_{x2} - Q_{x3} + N_{x4} = 0, \tag{6}$$

$$N_{x1} + Q_{x2} - N_{x3} - Q_{x4} = 0, \tag{7}$$

$$M_{x1} + M_{x2} + M_{x3} + M_{x4} = 0. \tag{8}$$

In Eqs. (6)–(8), Q_{xi} and M_{xi} represent the net vertical shear force and the bending moment, and are given by [9]

$$Q_{xi} = -D\left(\frac{\partial^3 w_i}{\partial x_i^3} + (2-v)\frac{\partial^3 w_i}{\partial x_i \partial y^2}\right), \tag{9}$$

$$M_{xi} = -D\left(\frac{\partial^2 w_i}{\partial x_i^2} + v\frac{\partial^2 w_i}{\partial y_i^2}\right). \tag{10}$$

Note that at the junction of the plates, Q_{xi} and M_{xi} in plate 1 are functions of w_{1II}^p. u_i is the in-plane longitudinal displacement in the x-direction. The in-plane longitudinal force N_{xi} can be written in terms of u_i using the impedance formula $u_i = -N_{xi}/\mathrm{j}\omega\rho h c_L$ [4], where for each plate, u_i is acting in the opposite direction to N_{xi}. c_L is the longitudinal wave speed and is given by $c_L = \sqrt{E/\rho(1-v^2)}$. For the L and T-shaped structures, the boundary conditions are obtained by eliminating components associated with the removed plates.

Using the boundary and continuity conditions, and the general solutions for the plate displacements described by Eq. (2), a matrix equation is obtained of the form $[\alpha_p][\mathbf{X}] = [\mathbf{F}_p]$. Eq. (11) represents the force matrix $[\mathbf{F}_p]$ for the cross-shaped plate.

$$[\mathbf{F}_p] = \left[0\ 0\ 0\ 0\ 0\ 0\ 0\ 0\ 0\ 0\ 0\ 0\ \frac{2F_p}{L_y}\sin k_y y_p\ \ 0\ 0\ 0\ 0\ 0\ 0\ 0\ 0\right]^{\mathrm{T}}. \tag{11}$$

A solution for the unknown coefficients of column vector $[\mathbf{X}]$ may be obtained by $[\mathbf{X}] = [\alpha_p]^{-1}[\mathbf{F}_p]$. $[\alpha_p]$ is a 20×20 matrix of the primary flexural displacement for the cross-shaped plate, and is given in Appendix A. In the $[\alpha_p]$ matrix, $k_L = \omega/c_L$ is the longitudinal wave number, where ω is the radian frequency.

3. Active control

A secondary point force of amplitude F_s is applied at a position on plate 1 corresponding to (x_s, y_s). The secondary flexural displacement can also be described by both a travelling wave solution in the x-direction and a modal solution in the y-direction. In the active control case, the general solution for the secondary displacement may be expressed as $w_i^s(x,y) = G_s F_s$ where $i =$ 1–4 for a cross-shaped plate, $i =$ 1–3 for a T-shaped plate, and $i =$ 1–2 for an L-shaped plate. G_s is the transfer function and is given by [10]

$$G_s = \sum_{m'=1}^{\infty} \frac{2}{L_y D}\sin(k_y y_s)[\alpha_s]_{n,12}^{-1}[E_i^s]\sin(k_y y). \tag{12}$$

$[\alpha_s]$ and $[\mathbf{F}_s]$ are the same as $[\alpha_p]$ and $[\mathbf{F}_p]$ except they are functions of mode number m', and x_p is replaced by x_s. As the secondary forcing matrix $[\mathbf{F}_s]$ has one non-zero element only, the inverse

matrix $[\alpha_s]^{-1}$ can be expressed using a single column of the matrix $[\alpha_s]$ [10]. For the cross-shaped plate, $[\alpha_s]^{-1}_{n,12}$ corresponds to the 12th column of the inverse matrix $[\alpha_s]^{-1}$ where $n = 1$–20 corresponds to the number of rows. For the cross-shaped plate, $[E_i^s]$ is described as

$$[E_{1I}^s] = [e^{-jk_x x_1} \; e^{jk_x x_1} \; e^{-k_n x_1} \; e^{k_n x_1} \; 0 \; 0 \; 0 \; 0 \; 0 \; 0 \; 0 \; 0 \; 0 \; 0 \; 0 \; 0 \; 0 \; 0 \; 0 \; 0]^T$$
$$x_s \leqslant x_1 \leqslant L_{x1}, \tag{13}$$

$$[E_{1II}^s] = [0 \; 0 \; 0 \; 0 \; e^{-jk_x x_1} \; e^{jk_x x_1} \; e^{-k_n x_1} \; e^{k_n x_1} \; 0 \; 0 \; 0 \; 0 \; 0 \; 0 \; 0 \; 0 \; 0 \; 0 \; 0 \; 0]^T$$
$$0 \leqslant x_1 \leqslant x_s, \tag{14}$$

$$[E_2^s] = [0 \; 0 \; 0 \; 0 \; 0 \; 0 \; 0 \; 0 \; e^{-jk_x x_2} \; e^{jk_x x_2} \; e^{-k_n x_2} \; e^{k_n x_2} \; 0 \; 0 \; 0 \; 0 \; 0 \; 0 \; 0 \; 0]^T$$
$$0 \leqslant x_2 \leqslant L_{x2}, \tag{15}$$

$$[E_3^s] = [0 \; 0 \; 0 \; 0 \; 0 \; 0 \; 0 \; 0 \; 0 \; 0 \; 0 \; 0 \; 0 \; e^{-jk_x x_3} \; e^{jk_x x_3} \; e^{-k_n x_3} \; e^{k_n x_3} \; 0 \; 0 \; 0 \; 0]^T$$
$$0 \leqslant x_3 \leqslant L_{x3}, \tag{16}$$

$$[E_4^s] = [0 \; 0 \; 0 \; 0 \; 0 \; 0 \; 0 \; 0 \; 0 \; 0 \; 0 \; 0 \; 0 \; 0 \; 0 \; 0 \; 0 \; e^{-jk_x x_4} \; e^{jk_x x_4} \; e^{-k_n x_4} \; e^{k_n x_4}]^T$$
$$0 \leqslant x_4 \leqslant L_{x4}. \tag{17}$$

It is also possible to describe the primary flexural displacement in terms of the primary force amplitude F_p and the primary transfer function G_p. The general solution for the primary displacement is given by $w_i^p(x, y) = G_p F_p$, where G_p is the same as G_s, except $[\alpha_s]$, $[E_i^s]$ and y_s are replaced with $[\alpha_p]$, $[E_i^p]$ and y_p, respectively. The total flexural displacement can be obtained by adding the plate displacement induced by the primary force and the secondary flexural waves generated by the control source:

$$w_i^T(x_i, y) = w_i^p(x_i, y) + w_i^s(x_i, y). \tag{18}$$

A cost function is developed using a feedforward adaptive least-mean-square algorithm [11]. The cost function to be minimized is the total squared plate displacement at an error sensor location (x_{ei}, y_e). In order to minimize the total squared plate displacement, the cost function is expressed as a quadratic function in terms of the control force [11]

$$w_i^T (w_i^T)^* = F_s A_\Pi F_s^* + F_s^* B_\Pi F_p + F_s B_\Pi^* F_p^* + F_p^* C_\Pi F_p, \tag{19}$$

where the asterisk '*' denotes the complex conjugate. Due to orthogonal relationships of modes, $A_\Pi = G_s G_s^*$ is a function of the mode number m', $B_\Pi = G_s^* G_p$ and $C_\Pi = G_p^* G_p$ are functions of mode number m. The optimal control force that results in the minimization of the cost function is determined by setting to zero the partial derivatives of the cost function with respect to the real and imaginary parts of the control force [11]. It can be seen that the resulting optimal control force that results in the minimum squared plate displacement is given by

$$F_s|_{opt} = -F_p \frac{B_\Pi}{A_\Pi}. \tag{20}$$

4. Results and discussion

The material of the rectangular plates investigated was chosen as aluminium with a density $\rho = 2700\,\mathrm{kg/m^3}$, Young's modulus $E = 7.1 \times 10^{10}\,\mathrm{N/m^2}$ and Poisson's ratio $v = 0.3$. The internal distributed damping in the structure was accounted for in the analytical modelling by including the complex Young's modulus using $E(1 + j\eta)$, where $\eta = 0.001$ is the structural loss factor. Each plate has a length and width of 0.6 and 0.5 m, respectively, and a thickness of 2 mm. The primary response was initially examined in order to determine the modeshapes at the resonance frequencies. To obtain the frequency responses of the L, T and cross-shaped plates, the primary shaker was placed on plate 1 at a location of $(x_p, y_p) = (0.618L_{x1}, 0.618L_y) = (0.371\,\mathrm{m}, 0.31\,\mathrm{m})$, which results in simultaneous excitation of all the structural modes. For the active control of the L, T and cross-shaped plates, the primary and control forces were always located in close proximity on plate 1, and the error sensor was placed on the adjacent plates on an anti-nodal position.

In order to investigate the effect of active control on the global response of the plates, different modes of vibration were examined. For the L, T and cross-shaped plates, the uncontrolled and controlled responses for two modes of vibration were investigated. All forcing and error sensor positions are given in metres. For the L-shaped plate, the two modes of vibration were examined at resonance frequencies of 202.95 and 224.89 Hz, as shown in Figs. 2(a) and 3(a) respectively. At 202.95 Hz, the modeshape has two nodal lines running along the x-direction, whereas the second modeshape at 224.89 Hz has only one nodal line running along the x-direction at the midway point in the y-direction ($y = 0.25\,\mathrm{m}$). Fig. 2(b) shows the controlled response at the resonance frequency of 202.95 Hz, for a control force location of $(x_s, y_s) = (0.371, 0.19)$ on plate 1. This control location corresponds to the same x-location as the primary force, and is symmetrical with the primary force along the y-direction. The location of the control force on plate 1 remained fixed, and was also used for the T and cross-shaped plates. The error sensor was positioned on plate 2 at $(x_{e2}, y_e) = (0.2, 0.25)$, which corresponds to an anti-nodal location and is also midway

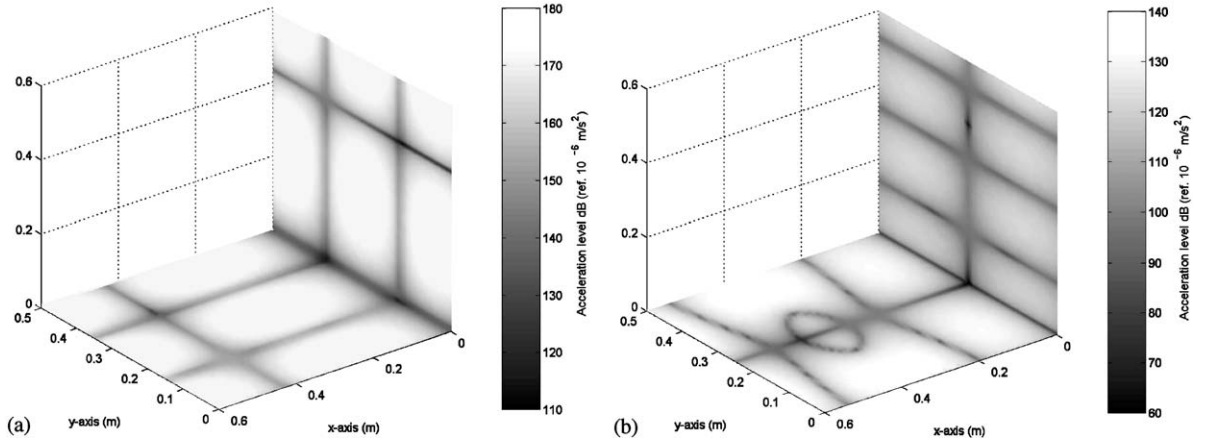

Fig. 2. (a) Contour plot of the modeshape at 202.95 Hz for the L-shaped plate. 2(b) Contour plot of the controlled response at 202.95 Hz and an error sensor location of $(x_{e2}, y_e) = (0.2, 0.25)$.

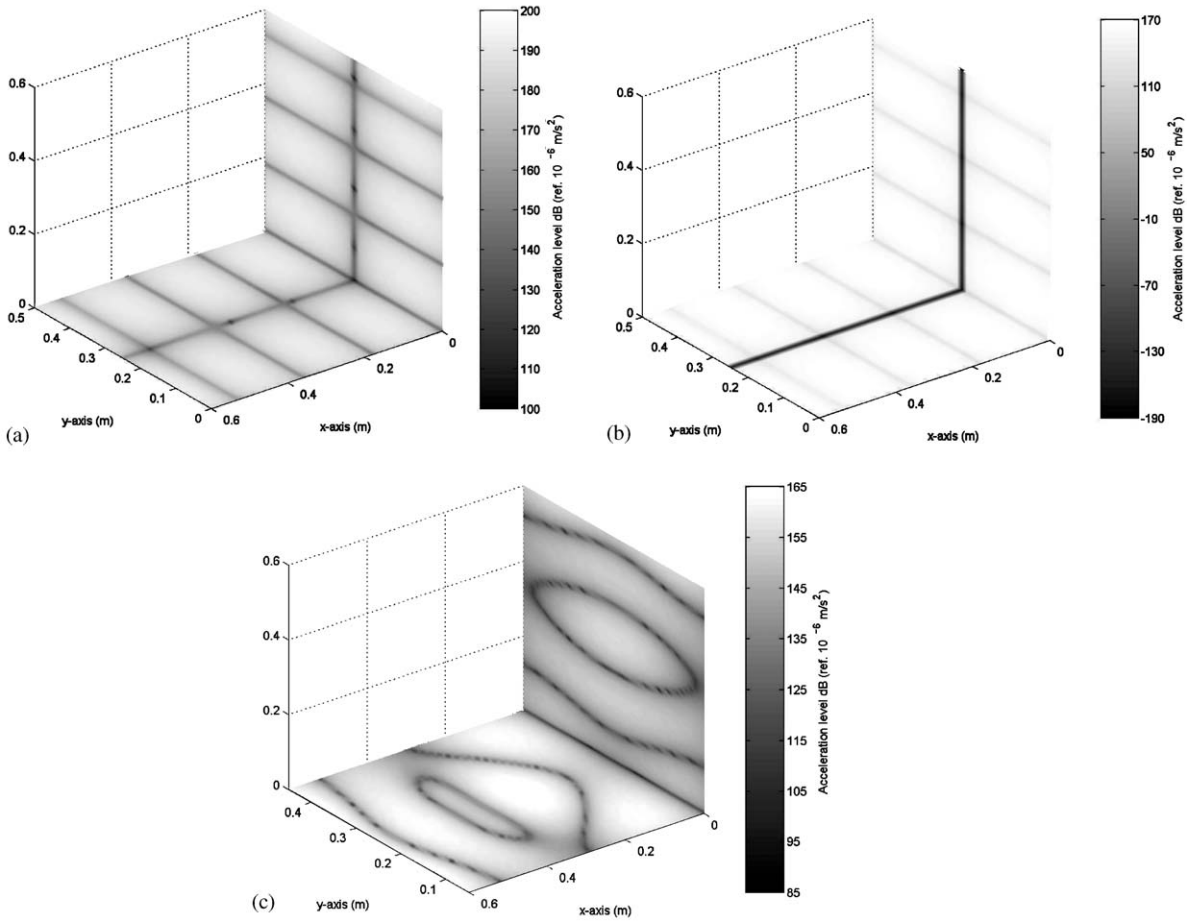

Fig. 3. (a) Contour plot of the modeshape at 224.89 Hz for the L-shaped plate. (b) Contour plot of the controlled response at 224.89 Hz and an error sensor location of $(x_{e2}, y_e) = (0.3, 0.25)$. (c) Contour plot of the controlled response at 224.89 Hz and an error sensor location of $(x_{e2}, y_e) = (0.3, 0.125)$.

between and downstream of the primary and control actuators. Fig. 2(b) shows that global attenuation in both plates is achieved, with up to 45dB attenuation at the anti-nodal locations. The same attenuation levels were achieved when the error sensor was positioned at any x-location and $y_e = 0.25$, that is, the control performance is independent of the x-location for an error sensor at the midway point in the y-direction. This result was also confirmed when the error sensor was located at $(x_{e2}, y_e) = (0.425, 0.25)$ which corresponds to a nodal line at an x-location. The optimal control performance, which occurs when the modeshape has an anti-nodal line along the x-direction at the midway point of $y = 0.25$ in the y-direction, is attributed to the symmetrical arrangement of the control force and the error sensor with respect to the primary force location. At error sensor locations away from $y_e = 0.25$, the control performance was shown to deteriorate. When the error sensor was located at the intersection of a nodal point in both the x- and y-directions, for example, at $(x_{e2}, y_e) = (0.425, 0.34)$, no attenuation of the uncontrolled response was achieved. For the frequency of 224.89 Hz, the error sensor was located on the nodal line at

$(x_{e2}, y_e) = (0.3, 0.25)$, and at an anti-nodal location of $(x_{e2}, y_e) = (0.3, 0.125)$. Fig. 3(b) shows that when the error sensor was positioned on a nodal line at $(x_{e2}, y_e) = (0.3, 0.25)$, attenuation is only achieved along the nodal line at $y = 0.25$ m, and corresponds to the midway point in the y-direction. The significant attenuation at $y = 0.25$ m is again attributed to the symmetrical arrangement of the primary and control application. When the error sensor was located on an anti-nodal position of $(x_{e2}, y_e) = (0.3, 0.125)$, global attenuation of around 40 dB is achieved (Fig. 3c).

For the T-shaped structure, resonance frequencies of 152.12 and 203.05 Hz were examined, and Figs. 4(a) and 5(a), respectively, show the contour plots of the uncontrolled responses. The first modeshape corresponding to a resonance frequency of 152.12 Hz has one nodal line running along the x-direction at $y = 0.25$ m, whereas the second resonance frequency of 203.05 Hz has two nodal lines running along the x-direction at $y = 0.15$ and 0.35 m. For the resonance frequency of 152.12 Hz, Figs. 4(b) and (c), respectively, show the controlled response when the error sensor was located along the nodal line at $(x_{e2}, y_e) = (0.35, 0.25)$, and at an anti-nodal position of $(x_{e2}, y_e) =$

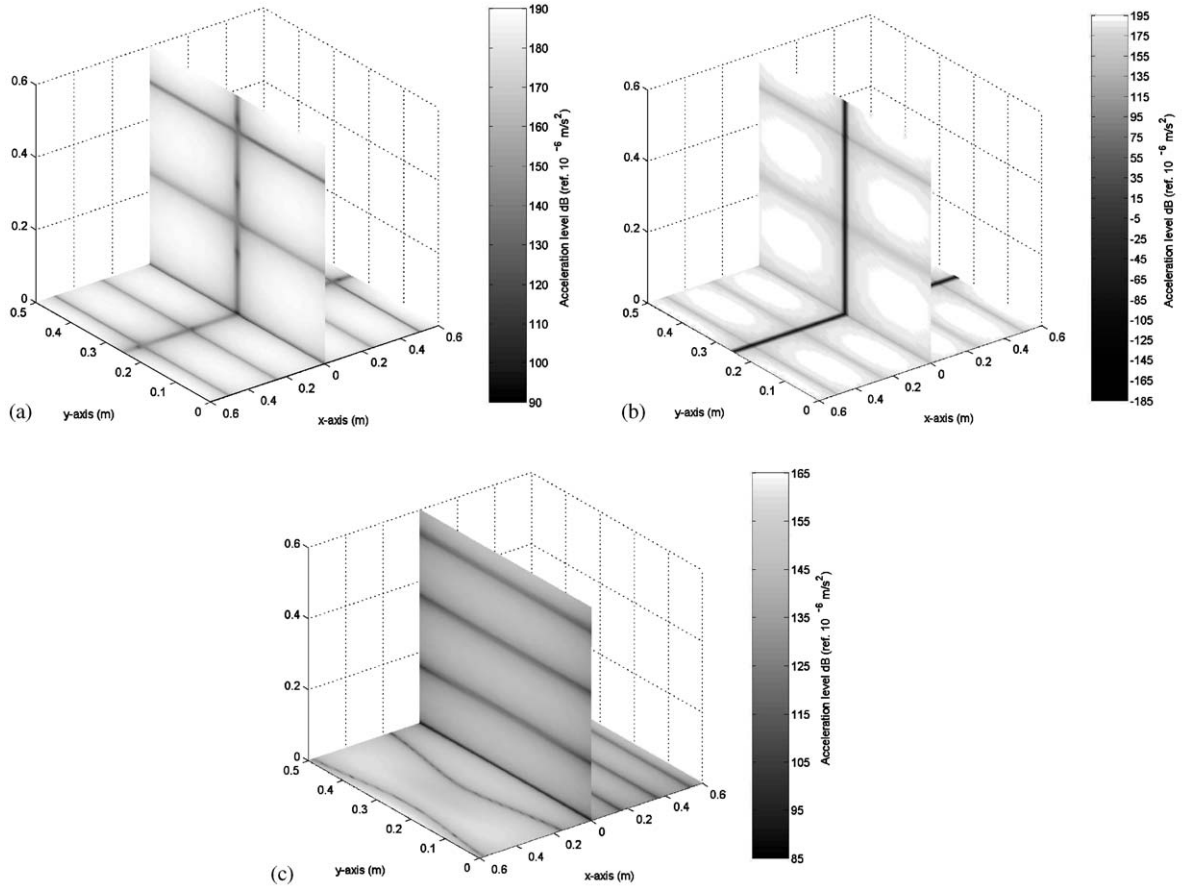

Fig. 4. (a) Contour plot of the modeshape at 152.12 Hz for the T-shaped plate. (b) Contour plot of the controlled response at 152.12 Hz and an error sensor location of $(x_{e2}, y_e) = (0.35, 0.25)$. (c) Contour plot of the controlled response at 152.12 Hz and an error sensor location of $(x_{e2}, y_e) = (0.4, 0.375)$.

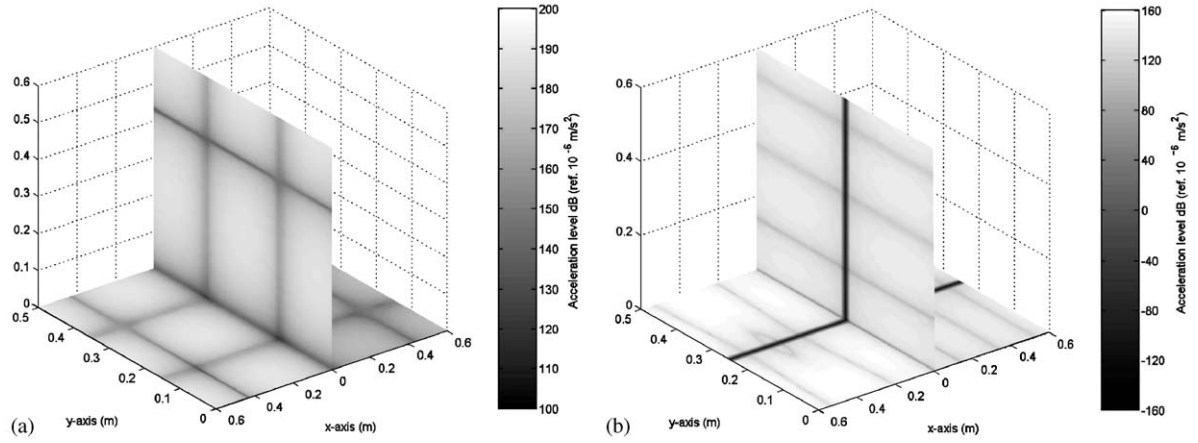

Fig. 5. (a) Contour plot of the modeshape at 203.05 Hz for the T-shaped plate. (b) Contour plot of the controlled response at 203.05 Hz and an error sensor location of $(x_{e2}, y_e) = (0.35, 0.25)$.

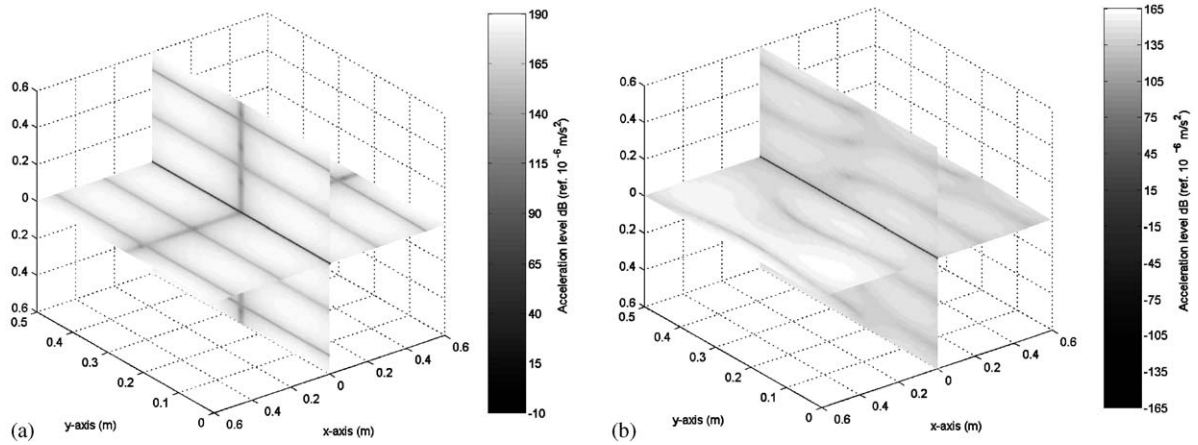

Fig. 6. (a) Contour plot of the modeshape at 151.99 Hz for the cross-shaped plate. (b) Contour plot of the controlled response at 151.99Hz and an error sensor location of $(x_{e3}, y_e) = (0.38, 0.125)$.

$(0.4, 0.375)$ on plate 2. Fig. 4(b) shows that the when the error sensor is located on the nodal line $y = 0.25$, attenuation is only achieved along the nodal line, and there is very little or no attenuation achieved elsewhere on the plates. Fig. 4(c) shows that global attenuation is achieved when the error sensor is positioned at an anti-nodal location of $(x_{e2}, y_e) = (0.4, 0.375)$ on plate 2. For the second resonance frequency of 203.05 Hz, the error sensor was located at an anti-nodal position in the x-direction of $(x_{e2}, y_e) = (0.35, 0.25)$, and global attenuation was achieved (Fig. 5(b)). Active control using a single control force and a single error sensor was also investigated for two modes of vibration for the cross-shaped plate. Figs. 6(a) and 7(a), respectively, show contour plots of the mode shapes for two resonance frequencies corresponding to 151.99 and 203.45 Hz. The 151.99 Hz modeshape has a single nodal line running along the x-direction at the midway point in the y-direction, and for the 203.45 Hz modeshape, there are

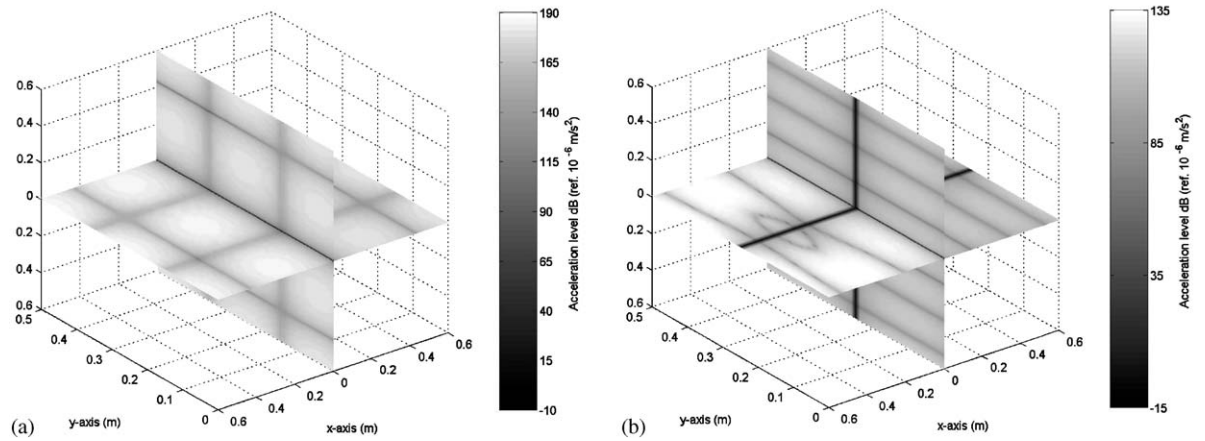

Fig. 7. (a) Contour plot of the modeshape at 203.45 Hz for the cross-shaped plate. (b) Contour plot of the controlled response at 203.45 Hz and an error sensor location of $(x_{e4}, y_e) = (0.3, 0.25)$.

two nodal lines running along the x-direction. For the natural frequency of 151.99 Hz, the error sensor was located at an anti-nodal position on plate 3 at $(x_{e3}, y_e) = (0.38, 0.125)$, and similarly, for 203.45 Hz, the error sensor was positioned on an anti-nodal line on plate 4 at $(x_{e4}, y_e) = (0.3, 0.25)$. The controlled responses for both frequencies are shown in Figs. 6(b) and 7(b). Fig. 6(b) shows that global attenuation levels in all four plates of around 35 dB was achieved. Fig. 7(b) also shows that global attenuation in all four plates is achieved, with attenuation levels of approximately 50 dB obtained at the anti-nodal locations. Global attenuation of this magnitude was also reached when the single error sensor was placed at anti-nodal locations on the other plates making up the cross-shaped structure. When the error sensor was moved away from the anti-nodal position, the control performance deteriorated.

5. Conclusions

An analytical and computational investigation of the dynamic response characteristics of a series of rectangular plates coupled together at right angles and subject to point force excitation has been conducted. The plate structures investigated included an L, T and cross-shaped configuration. Feedforward active control of the flexural waves in the plate configurations was investigated, and global attenuation was achieved using a single control force and a single error sensor located at an anti-nodal position. The attenuation achieved for the L, T and cross-shaped plates were strongly dependent on both the error sensor location and resonance frequency.

Acknowledgements

Financial support for this work from the Australian Research Council and the Australian Defence Science and Technology Organisation, Maritime Platforms Division is gratefully acknowledged.

Appendix A

$$
[\alpha_p] = \begin{bmatrix}
(-k_x^2 - vk_y^2)\mathrm{e}^{-\mathrm{j}k_x L_{x1}} & (-k_x^2 - vk_y^2)\mathrm{e}^{\mathrm{j}k_x L_{x1}} & (k_n^2 - vk_y^2)\mathrm{e}^{-k_n L_{x1}} & (k_n^2 - vk_y^2)\mathrm{e}^{k_n L_{x1}} & 0 \\
\mathrm{j}k_x(k_x^2 + (2-v)k_y^2)\mathrm{e}^{-\mathrm{j}k_x L_{x1}} & -\mathrm{j}k_x(k_x^2 + (2-v)k_y^2)\mathrm{e}^{\mathrm{j}k_x L_{x1}} & -k_n(k_n^2 - (2-v)k_y^2)\mathrm{e}^{-k_n L_{x1}} & k_n(k_n^2 - (2-v)k_y^2)\mathrm{e}^{k_n L_{x1}} & 0 \\
0 & 0 & 0 & 0 & 0 \\
0 & 0 & 0 & 0 & 0 \\
0 & 0 & 0 & 0 & 0 \\
0 & 0 & 0 & 0 & 0 \\
0 & 0 & 0 & 0 & 0 \\
0 & 0 & 0 & 0 & 0 \\
\mathrm{e}^{-\mathrm{j}k_x x_p} & \mathrm{e}^{\mathrm{j}k_x x_p} & \mathrm{e}^{-k_n x_p} & \mathrm{e}^{k_n x_p} & -\mathrm{e}^{-\mathrm{j}k_x x_p} \\
-\mathrm{j}k_x\mathrm{e}^{-\mathrm{j}k_x x_p} & \mathrm{j}k_x\mathrm{e}^{\mathrm{j}k_x x_p} & -k_n\mathrm{e}^{-k_n x_p} & k_n\mathrm{e}^{k_n x_p} & \mathrm{j}k_x\mathrm{e}^{-\mathrm{j}k_x x_p} \\
-k_x^2\mathrm{e}^{-\mathrm{j}k_x x_p} & -k_x^2\mathrm{e}^{\mathrm{j}k_x x_p} & k_n^2\mathrm{e}^{-k_n x_p} & k_n^2\mathrm{e}^{k_n x_p} & k_x^2\mathrm{e}^{-\mathrm{j}k_x x_p} \\
\mathrm{j}k_x^3\mathrm{e}^{-\mathrm{j}k_x x_p} & -\mathrm{j}k_x^3\mathrm{e}^{\mathrm{j}k_x x_p} & -k_n^3\mathrm{e}^{-k_n x_p} & k_n^3\mathrm{e}^{k_n x_p} & -\mathrm{j}k_x^3\mathrm{e}^{-\mathrm{j}k_x x_p} \\
0 & 0 & 0 & 0 & -\mathrm{j}k_x \\
0 & 0 & 0 & 0 & 0 \\
0 & 0 & 0 & 0 & 0 \\
0 & 0 & 0 & 0 & 1 \\
0 & 0 & 0 & 0 & 0 \\
0 & 0 & 0 & 0 & \mathrm{j}(k_x^3 + k_p^4/k_L) \\
0 & 0 & 0 & 0 & 0 \\
0 & 0 & 0 & 0 & -k_x^2 - vk_y^2
\end{bmatrix}
$$

$$
\begin{array}{ccccc}
0 & 0 & 0 & 0 & 0 \\
0 & 0 & 0 & 0 & 0 \\
0 & 0 & 0 & (-k_x^2 - vk_y^2)\mathrm{e}^{-\mathrm{j}k_x L_{x2}} & (-k_x^2 - vk_y^2)\mathrm{e}^{\mathrm{j}k_x L_{x2}} \\
0 & 0 & 0 & \mathrm{j}k_x(k_x^2 + (2-v)k_y^2)\mathrm{e}^{-\mathrm{j}k_x L_{x2}} & -\mathrm{j}k_x(k_x^2 + (2-v)k_y^2)\mathrm{e}^{\mathrm{j}k_x L_{x2}} \\
0 & 0 & 0 & 0 & 0 \\
0 & 0 & 0 & 0 & 0 \\
0 & 0 & 0 & 0 & 0 \\
0 & 0 & 0 & 0 & 0 \\
-\mathrm{e}^{\mathrm{j}k_x x_p} & -\mathrm{e}^{-k_n x_p} & -\mathrm{e}^{k_n x_p} & 0 & 0 \\
-\mathrm{j}k_x \mathrm{e}^{jk_x x_p} & k_n \mathrm{e}^{-k_n x_p} & -k_n \mathrm{e}^{k_n x_p} & 0 & 0 \\
k_x^2 \mathrm{e}^{\mathrm{j}k_x x_p} & -k_n^2 \mathrm{e}^{-k_n x_p} & -k_n^2 \mathrm{e}^{k_n x_p} & 0 & 0 \\
\mathrm{j}k_x^3 \mathrm{e}^{\mathrm{j}k_x x_p} & k_n^3 \mathrm{e}^{-k_n x_p} & -k_n^3 \mathrm{e}^{k_n x_p} & 0 & 0 \\
\mathrm{j}k_x & -k_n & k_n & \mathrm{j}k_x & -\mathrm{j}k_x \\
0 & 0 & 0 & -\mathrm{j}k_x & \mathrm{j}k_x \\
1 & 1 & 1 & 0 & 0 \\
0 & 0 & 0 & 1 & 1 \\
0 & 0 & 0 & 0 & 0 \\
-\mathrm{j}(k_x^3 - k_p^4/k_L) & -(k_n^3 - \mathrm{j}k_p^4/k_L) & (k_n^3 + \mathrm{j}k_p^4/k_L) & 0 & 0 \\
0 & 0 & 0 & \mathrm{j}(k_x^3 + k_p^4/k_L) & -\mathrm{j}(k_x^3 - k_p^4/k_L) \\
-k_x^2 - vk_y^2 & k_n^2 - vk_y^2 & k_n^2 - vk_y^2 & -k_x^2 - vk_y^2 & -k_x^2 - vk_y^2
\end{array}
$$

$$
\begin{array}{ccccc}
0 & 0 & 0 & 0 & 0 \\
0 & 0 & 0 & 0 & 0 \\
(k_n^2 - vk_y^2)\mathrm{e}^{-k_n L_{x2}} & (k_n^2 - vk_y^2)\mathrm{e}^{k_n L_{x2}} & 0 & 0 & 0 \\
-k_n(k_n^2 - (2-v)k_y^2)\mathrm{e}^{-k_n L_{x2}} & k_n(k_n^2 - (2-v)k_y^2)\mathrm{e}^{k_n L_{x2}} & 0 & 0 & 0 \\
0 & 0 & (-k_x^2 - vk_y^2)\mathrm{e}^{-\mathrm{j}k_x L_{x3}} & (-k_x^2 - vk_y^2)\mathrm{e}^{\mathrm{j}k_x L_{x3}} & (k_n^2 - vk_y^2)\mathrm{e}^{-k_n L_{x3}} \\
0 & 0 & \mathrm{j}k_x(k_x^2 + (2-v)k_y^2)\mathrm{e}^{-jk_x L_{x3}} & -\mathrm{j}k_x(k_x^2 + (2-v)k_y^2)\mathrm{e}^{\mathrm{j}k_x L_{x3}} & -k_n(k_n^2 - (2-v)k_y^2)\mathrm{e}^{-k_n L_{x3}} \\
0 & 0 & 0 & 0 & 0 \\
0 & 0 & 0 & 0 & 0 \\
0 & 0 & 0 & 0 & 0 \\
0 & 0 & 0 & 0 & 0 \\
0 & 0 & 0 & 0 & 0 \\
0 & 0 & 0 & 0 & 0 \\
k_n & -k_n & 0 & 0 & 0 \\
-k_n & k_n & \mathrm{j}k_x & -\mathrm{j}k_x & k_n \\
0 & 0 & -\mathrm{j}k_x & \mathrm{j}k_x & -k_n \\
0 & 0 & 1 & 1 & 1 \\
1 & 1 & 0 & 0 & 0 \\
0 & 0 & -\mathrm{j}(k_x^3 - k_p^4/k_L) & \mathrm{j}(k_x^3 + k_p^4/k_L) & (k_n^3 + \mathrm{j}k_p^4/k_L) \\
-(k_n^3 - \mathrm{j}k_p^4/k_L) & (k_n^3 + \mathrm{j}k_p^4/k_L) & 0 & 0 & 0 \\
k_n^2 - vk_y^2 & k_n^2 - vk_y^2 & -k_x^2 - vk_y^2 & -k_x^2 - vk_y^2 & k_n^2 - vk_y^2
\end{array}
$$

$$
\begin{bmatrix}
0 & 0 & 0 & 0 & 0 \\
0 & 0 & 0 & 0 & 0 \\
0 & 0 & 0 & 0 & 0 \\
0 & 0 & 0 & 0 & 0 \\
(k_n^2 - vk_y^2)\mathrm{e}^{k_n L_{x3}} & 0 & 0 & 0 & 0 \\
k_n(k_n^2 - (2-v)k_y^2)\mathrm{e}^{k_n L_{x3}} & 0 & 0 & 0 & 0 \\
0 & (-k_x^2 - vk_y^2)\mathrm{e}^{-\mathrm{j}k_x L_{x4}} & (-k_x^2 - vk_y^2)\mathrm{e}^{\mathrm{j}k_x L_{x4}} & (k_n^2 - vk_y^2)\mathrm{e}^{-k_n L_{x4}} & (k_n^2 - vk_y^2)\mathrm{e}^{k_n L_{x4}} \\
0 & \mathrm{j}k_x(k_x^2 + (2-v)k_y^2)\mathrm{e}^{-\mathrm{j}k_x L_{x4}} & -\mathrm{j}k_x(k_x^2 + (2-v)k_y^2)\mathrm{e}^{\mathrm{j}k_x L_{x4}} & -k_n(k_n^2 - (2-v)k_y^2)\mathrm{e}^{-k_n L_{x4}} & k_n(k_n^2 - (2-v)k_y^2)\mathrm{e}^{k_n L_{x4}} \\
0 & 0 & 0 & 0 & 0 \\
0 & 0 & 0 & 0 & 0 \\
0 & 0 & 0 & 0 & 0 \\
0 & 0 & 0 & 0 & 0 \\
0 & 0 & 0 & 0 & 0 \\
-k_n & 0 & 0 & 0 & 0 \\
k_n & jk_x & -jk_x & k_n & -k_n \\
1 & 0 & 0 & 0 & 0 \\
0 & 1 & 1 & 1 & 1 \\
-(k_n^3 - \mathrm{j}k_p^4/k_L) & 0 & 0 & 0 & 0 \\
0 & -\mathrm{j}(k_x^3 - k_p^4/k_L) & \mathrm{j}(k_x^3 + k_p^4/k_L) & (k_n^3 + \mathrm{j}k_p^4/k_L) & -(k_n^3 - \mathrm{j}k_p^4/k_L) \\
k_n^2 - vk_y^2 & -k_x^2 - vk_y^2 & -k_x^2 - vk_y^2 & k_n^2 - vk_y^2 & k_n^2 - vk_y^2
\end{bmatrix}
$$

References

[1] J. Kim, H. Kim, H. Kang, S. Kim, Effects of inplane modes in SEA on structure-borne noise transmission in ship structures, Proceedings of the Fourth International Congress of Sound and Vibration, St. Petersburg, Russia, 1996, pp. 217–222.
[2] Y. Shen, B.M. Gibbs, An approximate solution for the bending vibrations of a combination of rectangular thin plates, Journal of Sound and Vibration 105 (1986) 73–90.
[3] S.V. Budrin, A.S. Nikiforov, Wave transmission through assorted plate joints, Soviet Physics-Acoustics 9 (1964) 333–336.
[4] L. Cremer, M. Heckl, E.E. Ungar, Structure-Borne Sound, 2nd Edition, Springer, Berlin, 1988.
[5] P.G. Craven, B.M. Gibbs, Sound transmission and mode coupling at junctions of thin plates, Part I: representation of the problem, Journal of Sound and Vibration 77 (1981) 417–427.
[6] C. Boisson, J.L. Guyader, P. Millot, C. Lesuer, Energy transmission in finite coupled plates, Part II: application to an L shaped structure, Journal of Sound and Vibration 81 (1982) 93–105.
[7] R.S. Langley, K.H. Heron, Elastic wave transmission through plate/beam junctions, Journal of Sound and Vibration 143 (1990) 241–253.
[8] N.J. Kessissoglou, Active attenuation of the wave transmission through an L-plate junction, Journal of the Acoustical Society of America 110 (2001) 267–277.
[9] S. Timoshenko, S. Woinowsky-Krieger, Theory of Plates and Shells, 2nd Edition., McGraw-Hill, Inc., New York, 1959.
[10] X. Pan, C.H. Hansen, Active control of vibratory power transmission along a semi-infinite plate, Journal of Sound and Vibration 184 (1995) 585–610.
[11] C.R. Fuller, S.J. Elliott, P.A. Nelson, Active Control of Vibration, Academic Press, London, 1996.